PAPER

Quantification of low affinity binding interactions between natural killer cell inhibitory receptors and targeting ligands with a self-induced back-action actuated nanopore electrophoresis (SANE) sensor

IOP Publishing Nanotechnology

Nanotechnology **32** (2021) 045501 (17pp) https://doi.org/10.1088/1361-6528/abbf26

Quantification of low affinity binding interactions between natural killer cell inhibitory receptors and targeting ligands with a self-induced back-action actuated nanopore electrophoresis (SANE) sensor

Sai Santosh Sasank Peri[1], Manoj Kumar Sabnani[2], Muhammad Usman Raza[1], Elizabeth L Urquhart[3], Soroush Ghaffari[2], Jung Soo Lee[4], Min Jun Kim[4], Jon Weidanz[2] and George Alexandrakis[3]

[1] Department of Electrical Engineering, University of Texas at Arlington, Arlington, TX, United States of America
[2] Department of Biology, University of Texas at Arlington, Arlington, TX, United States of America
[3] Department of Bioengineering, University of Texas at Arlington, Arlington, TX, United States of America
[4] Department of Mechanical Engineering, Southern Methodist University, Dallas, TX, United States of America

E-mail: galex@uta.edu

Received 10 August 2020, revised 29 September 2020
Accepted for publication 7 October 2020
Published 28 October 2020

Abstract

A plasmonic nanopore sensor enabling detection of bimodal optical and electrical molecular signatures was fabricated and tested for its ability to characterize low affinity ligand-receptor interactions. This plasmonic nanosensor uses self-induced back-action (SIBA) for optical trapping to enable SIBA-actuated nanopore electrophoresis (SANE) through a nanopore located immediately below the optical trap volume. A natural killer (NK) cell inhibitory receptor heterodimer molecule CD94/NKG2A was synthesized to target a specific peptide-presenting Qa-1^b Qdm ligand as a simplified model of low-affinity interactions between immune cells and peptide-presenting cancer cells that occurs during cancer immunotherapy. A cancer-irrelevant Qa-1^b GroEL ligand was also targeted by the same receptor as a control experiment to test for non-specific binding. The analysis of different pairs of bimodal SANE sensor signatures enabled discrimination of ligand, receptor and their complexes and enabled differentiating between specific and non-specific ligand interactions. We were able to detect ligand-receptor complex binding at concentrations over 500 times lower than the free solution equilibrium binding constant (K_D). Additionally, SANE sensor measurements enabled estimation of the fast dissociation rate (k_{off}) for this low-affinity specific ligand-receptor system, previously shown to be challenging to quantify with commercial technologies. The k_{off} value of targeted peptide-presenting ligands is known to correlate with the subsequent activation of immune cells *in vivo*, suggesting the potential utility of the SANE senor as a screening tool in cancer immunotherapy.

Keywords: solid-state nanopore, dual nanohole, plasmonics, dual modality nanosensing, receptor ligand interactions, binding kinetics, cancer immunotherapy

(Some figures may appear in colour only in the online journal)

Introduction

Single molecule detection methods have been able to quantify protein-ligand interactions and provide valuable information that is usually unavailable from ensemble methods such as ELISA, surface plasmon resonance (SPR) and other assays [1]. These modalities have utilized either optical or electrical sensing technologies to differentiate between bound and unbound reactants. Current single molecule interaction analysis methods utilizing optical technologies include optical tweezers, atomic force microscopy, single molecule FRET and ultra-high resolution microscopy [2]. Electrical sensors for single molecule analysis predominantly consist of solid-state nanopores (SSNPs) [3] and electrical break junctions [4], of which the former are more popular due to their sensitivity and specificity.

SSNPs are nanometer sized pores milled in suspended dielectric membranes using focused ion beam (FIB) [5] or transmission electron microscopy [6] and work as a robust alternative to biological pores [7]. In nanopore sensing, two compartments filled with electrolyte solution are joined with the SSNP at its center. Analyte molecules are added to one compartment and translocated through the SSNP into the other using applied bias. The translocation of the molecule causes changes in the ionic current signatures that define the data metrics (i.e. translocation current and translocation time). Translocation behavior of the molecules are dependent on molecular size, volume and surface charge [8], as well as solution pH and salt concentrations [9]. SSNPs have been used to study and characterize biomolecular interactions [10–16].

On the optical sensing side, an area of focus in recent years has been the development of metallic nanoaperture structures that utilize strong plasmonic confinement to enable using self-induced back action (SIBA) as a mechanism for the optical trapping of protein-size molecules at low laser powers (approximately 0.7 mW) [17, 18]. Metallic nanoapertures circumvent the difficulty of using high laser powers to trap entities smaller than 100 nm with optical tweezers [19]. SIBA-based optical trapping has been reported to quantify protein-small molecule interactions by trapping the molecules in a double nanohole (DNH) structure milled in a gold (Au) film on a glass substrate [20–22]. However, optical sensor throughput can be limited by long optical trapping times and diffusion-limited molecular transport to the sensing region, as many experiments often use low analyte concentrations. Plasmonic nanopore structures have been previously suggested as a means of using optical illumination to create local heating on plasmonic nanoantennas to augment event detection rate through an SSNP located immediately below [23, 24].

Recently, we [25, 26] and others [1, 27–30] have reported on plasmonic nanopores combining the optical trapping of metallic nanoapertures with the electrical sensing of SSNPs to augment optical event detection rate with the help of an external electrical bias, while also slowing down SSNP event detection by use of the spatially overlapping optical trapping field. In our prior work [25], a DNH nanoaperture had an SSNP placed at its center, which enabled the combination of optical trapping by SIBA with electrical nanopore sensing. The resulting bimodal sensor technology was named as a SIBA-actuated nanopore electrophoresis (SANE). The DNH was milled by neon (Ne) ion FIB and had tapered walls that excited the wedge plasmons such that the molecule was trapped above the mouth of the SSNP. In initial experiments, the presence of the optical trap near the SSNP extended the translocation time of nanoparticles up to four orders of magnitude compared to a classical nanopore [3]. In our subsequent work, we detected high affinity antibody-ligand interactions using the bimodal optical-electrical data from the SANE sensor where we were able to identify the individual proteins, their protein complexes, as well as the specific and non-specific binding interactions [26]. A major finding of that work was the SANE sensor enabled the formation and subsequent detection of a much higher antibody-ligand complex bound fraction compared to that expected for corresponding bulk solution concentrations.

The purpose of this work is to go beyond the initial nanoparticle tests and high-affinity interaction measurements, and demonstrate the ability of the SANE sensor to quantify low-affinity interactions, which is challenging to do with existing commercial technologies [31]. Moreover, the proteins used in this work represent a simplified model of ligand-receptor interactions that are relevant to cancer immunotherapy. CD94 and NKG2A heterodimer receptors are expressed on the cell surface of natural killer (NK) lymphocyte cells [32]. These receptors can be cloned and expressed in a mammalian expression system as a soluble recombinant protein, CD94/NKG2A heterodimer (henceforth referred to as NK receptor). The NK receptor can recognize a specific peptide-presenting major histocompatibility complex (pMHC) ligand known as Qdm/Qa-1^b (henceforth referred to as Qdm) [33], which we use as the specific target ligand in this work. Usually, expression of the Qdm ligand is associated with an inhibitory response from the receptors on the NK cells. Tumor cells are also known to express the Qdm ligand to evade an immune system response as, in the absence of inhibitory ligands, the NK cells can kill the tumor cells [34]. Cancer-irrelevant ligands (GroEL) were also used in control experiments. GroEL is an immunodominant epitope expressed by Salmonella typhimurium and presented by a Qa-1^b MHC molecule. It is specifically recognized by CD8 + cytotoxic T lymphocytes after natural infection in the mouse [35, 36].

The SANE sensor bimodal signatures were tested for their ability to discriminate between individual ligands, receptors, and specific (Qdm-NK receptor) and non-specific (GroEL-NK receptor) receptor-ligand interactions in equimolar mixtures over a wide range of concentrations. We also tested the ability of the SANE sensor to detect receptor-ligand complexes at concentrations much lower than K_D for these low-affinity interactions. Furthermore, the low affinity of NK receptors to the human analogue of Qdm resulted in short binding times that were challenging to quantify in prior SPR experiments, as documented [37, 38]. Nevertheless, quantification of short binding times (k_{off} values measured in few

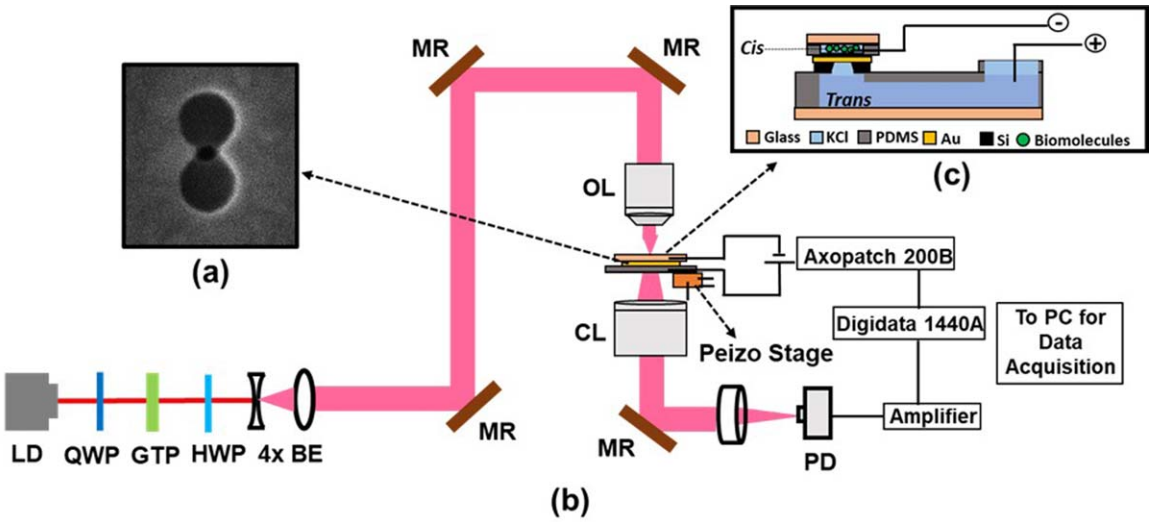

Figure 1. (a) Scanning electron microscope image of FIB-milled DNH and nanopores structure on the metal-dielectric membrane. (b) Experimental setup with optical and electrical measurement instruments. LD: Laser Diode, QWP: Quarter Wave Plate, GTP: Glan-Thompson Polarizer, HWP: Half Wave Plate, 4× BE: 4× Beam Expander, MR: Mirror, OL: Carl-Zeiss 1.3 N.A. 63× Objective Lens, CL: Condenser Lens, PD: Photodiode. (c) PDMS flow cell cross-sectional view with SANE sensor.

sec, or less) is well within the capability of the SANE sensor, and its measurement of k_{off} was consistent with scant information available in the literature for the Qdm-NK [38].

Materials and methods

SANE sensor fabrication

The SANE sensor was fabricated according to a previously reported procedure [25]. This sensor consists of a metal-dielectric membrane with nanostructures milled using FIB on a double-sided polished 4 inch silicon (Si) wafer (100 orientation). A 500 nm thick silicon dioxide (SiO_2) on the wafer was grown by thermal oxidation, followed by deposition of a 60 nm thick stoichiometric silicon nitride (Si_3N_4), henceforth referred to as SiN, layer by low pressure chemical vapor deposition on both sides of the Si wafer. On one side of the wafer (referred to as backside), square windows of side 786 μm were patterned using photolithography process. The SiN layer exposed in these windows was etched away using deep reactive ion etching with tertrafluoromethane (CF_4) gas at an etch rate of 1 nm min^{-1}, followed by etching of the SiO_2 layer using 6:1 buffered hydrofluoric (BHF). The underlying Si layer was etched anisotropically using a 22% tetramethylammonium hydroxide (TMAH) solution at 90 °C to create a 100 μm window on the front side, leaving SiN/SiO_2 layers suspended. On the front side, two thin film layers, a 5 nm chromium (Cr) layer, followed by 100 nm Au, were deposited through an e-beam evaporation method at a 0.1 nm s^{-1} deposition rate, where Cr was used as an adhesion layer for Au. Using a photolithography process, alignment markers were patterned on this Au side to assist in FIB milling. The Au and Cr layers in these marker regions were etched away using respective wet etchants (Sigma Aldrich). The Si wafer was diced into individual chips and the backing SiO_2 layer was etched using 6:1 BHF for each chip. These Si chips with a metal-dielectric membrane were placed inside a GFIS FIB (Carl Zeiss, ORION Nanofab, Peabody, MA) ultra-high vacuum chamber to mill the nanostructures. A DNH nanoaperture (100 nm diameter circles) was milled through the Au layer with tapered edges having a 15%–18% slope for optimal plasmon excitation [39]. In the SiN layer, a 25 nm diameter nanopore was milled using a Ne ion beam such that it was exactly at the middle of the DNH.

Experimental setup

Figure 1(a) shows a scanning electron microscope image of the milled DNH and nanopore structures comprising the SANE sensor. Figure 1(b) shows the schematic of the experimental setup, which was similar to our previously reported work [25]. Briefly, a near infrared region laser diode (820 nm, L820P200, Thorlabs) was collimated and circularly polarized using a QWP (WPQ05M, Thorlabs) to create a 2 mm diameter beam. This beam was linearly polarized using a Glan–Thompson linear polarizer (GTH10M, Thorlabs). An adjustable HWP (WPH05M, Thorlabs) was used to select the polarization that was parallel to the horizontal axis of the DNH for optimal excitation of wedge plasmons. The beam was expanded using a 4× beam expander (Newport) and passed through a periscope to the back aperture of a 63× oil immersion objective lens (NA = 1.3, Zeiss C-Apochromat). The light beam was focused through a cover slip onto the SANE chip. The chip was enclosed in a transparent PDMS flow cell (figure 1(b)), fabricated as per previously reported procedure [25]. This PDMS flow cell was attached to a piezo stage (MDT6938, Thorlabs) to perform coarse and fine adjustments and align the short axis of the DNH with the polarization of the laser beam. A condenser lens was used to collect the transmitted light from the DNH and then focus it onto a photodiode (PDA36A, Thorlabs). The PDMS flow cell

consisted of two chambers, one above the SANE sensor chip (*cis*) and the other below the chip (*trans*). Analytes mixed in 150 mM potassium chloride (KCl) solution were added to the *cis* chamber. Similar-molarity, KCl-only solution was added to the *trans* chamber. Two silver electrodes were immersed in bleach solution to form a coating of silver chloride (Ag/AgCl). One electrode was inserted in the *cis* and one in the *trans* chamber.

The electrodes were connected to an Axon Axopatch 200B patch clamp amplifier and digitizer equipment (Molecular Devices) through Axon Headstage (CV 203BU) and operated in voltage clamp mode. The change in resistance across the chambers was measured as a drop in ionic current flow when a protein passed through the nanopore while translocating from *cis* to *trans*. A faraday cage was built with aluminum foil (Reynolds) around the piezo-stage with the PDMS flow cell to eliminate low-frequency electromagnetic noise while recording the ionic current traces. Protein translocation events were performed at 100 mV voltage bias across the nanopore.

Generation of ligand and receptor molecules

Qa-1^{b} Qdm ligand (Qdm) [34], an MHC class Ib allotype from C57Blk/6 (mouse strain) analogous to HLA-E (Human), consisted of a purified mouse MHC I heavy chain Qa-1^{b} (35 kDa) and a human β2m (13 kDa) light chain. The peptide AMAPRTLLL (1 kDa) was derived from leader sequence of H2D^{b} and synthesized by Genescript, Piscataway, NJ and refolded *in vitro* to create a peptide-presenting MHC (pMHC) antigen that was purified by size exclusion chromatography [40]. This Qdm peptide is known to induce a NK cell inhibitory response when presented by Qa-1^{b} in the mouse [32, 33]. CD94 (~26 kDa) and NKG2A (~43 kDa) were cloned from murine NK cells and expressed as a soluble recombinant protein in mammalian plasmid in HEK293 cells. The CD94/NKG2A heterodimers specifically recognize Qdm/Qa-1^{b} pMHCs to form complexes [34]. Another ligand containing a different peptide, GroEL (refolded in Qa-1^{b} similar to Qdm) [35, 36] was used as negative control. The plasmid construct was a generous gift from AbeXXa Biologics Inc., while Dr Weidanz's group made the Qdm ligand (~45 kDa), GroEL ligand (~45 kDa) and the receptors (~150 kDa) in-house.

Sample preparation

To study the ligand-receptor interactions, stock solutions of ligands (Qdm/Qa-1^{b} or GroEL/Qa-1^{b}) and receptors (CD94/NKG2A) were mixed in equimolar concentrations of 1200, 600, 200 and 20 nM in separate experiments and incubated to react for about 30 min. The reacted mixtures were diluted in a KCl electrolyte (buffered at pH ~7.4, 150 mM) to achieve dilutions of 600, 300, 100 and 10 nM range. About 70 μl of sample solution was dispensed onto the *cis* side reservoir of the sensor. The *trans* reservoir was filled with 1.5 ml of 7.4 pH, 150 mM KCl solution.

Experimental data acquisition and analysis

We utilized our previously reported data acquisition and analysis methodology [26]. Briefly, the optical signals were detected using a photodiode (PDA36A, Thorlabs), and electrical signals were acquired using Axopatch 200 B (Molecular Devices). Both these signals were digitally processed through an analog-to-digital converter, Axon Digidata 1440 ADC, connected to a computer, where Axon pCLAMP 10.6 software was used for recording and analysis. Optical signals were recorded as changes in transmission amplitude proportional (step increases in voltage (optical transmission (V)) to the size of the particle in the optical trap. Optical-based metrics were calculated from the optical signals as percentage change in optical amplitude (optical step change) from the baseline and total trapping duration (optical trap time) for events where a positive step change (entering trap) was followed by a negative step change (leaving trap). Electrical signals were recorded as amplitude changes in the ionic current proportional to the charge and volume of the particles. These signals were filtered by a low pass 20 Hz eight-pole Bessel filter to remove high frequency noise. Electrical-based metrics calculated from these concurrent ionic current traces were the drop in current amplitude relative to baseline (translocation current) and the full width half-maximum of the current drop trace (translocation time). These concurrently acquired bimodal metrics were used in this work to characterize protein interactions.

Statistical analyses

We tested the differences in bimodal optical-electrical data types between unbound proteins (ligand versus receptor) as well as specific versus non-specific binding events (Qdm ligand-NK receptor versus GroEL-NK receptor mixtures) using two-sample, two-dimensional Kolmogorov-Smirnov (2s–2d KS) tests in MATLAB, with p-value significance set at 0.01 [26]. We used an independent samples t-test to evaluate the differences in the unimodal optical and electrical data types between individual proteins and their mixtures, with p-value significance set at 0.05.

Identification of ligand-receptor complexes in a mixture was based on optical step change magnitude threshold [41] that was applied consistently across all experiments. This threshold was identified by first compiling optical step change data into histograms and fitting three Gaussian curves to identify the ligand, receptor, and complex populations (Mathematica). Then, the ligand-receptor optical step threshold was selected as the point of minimum overlap between histograms of unbound receptors and likely bound complexes.

Furthermore, the use of bound Qdm-NK receptor complex threshold enabled subsequent estimation of the bound fraction (BF) in SANE sensor experiments as $\mathrm{BF} = [\mathrm{Qdm-K\ \ receptor}]/([\mathrm{Qdm}] + [\mathrm{Qdm-K\ \ receptor}])$, where square brackets indicate molar concentrations. We also estimated the free solution BF based on the reported value of K_D for Qdm ligands interacting with a CD94/NKG2A

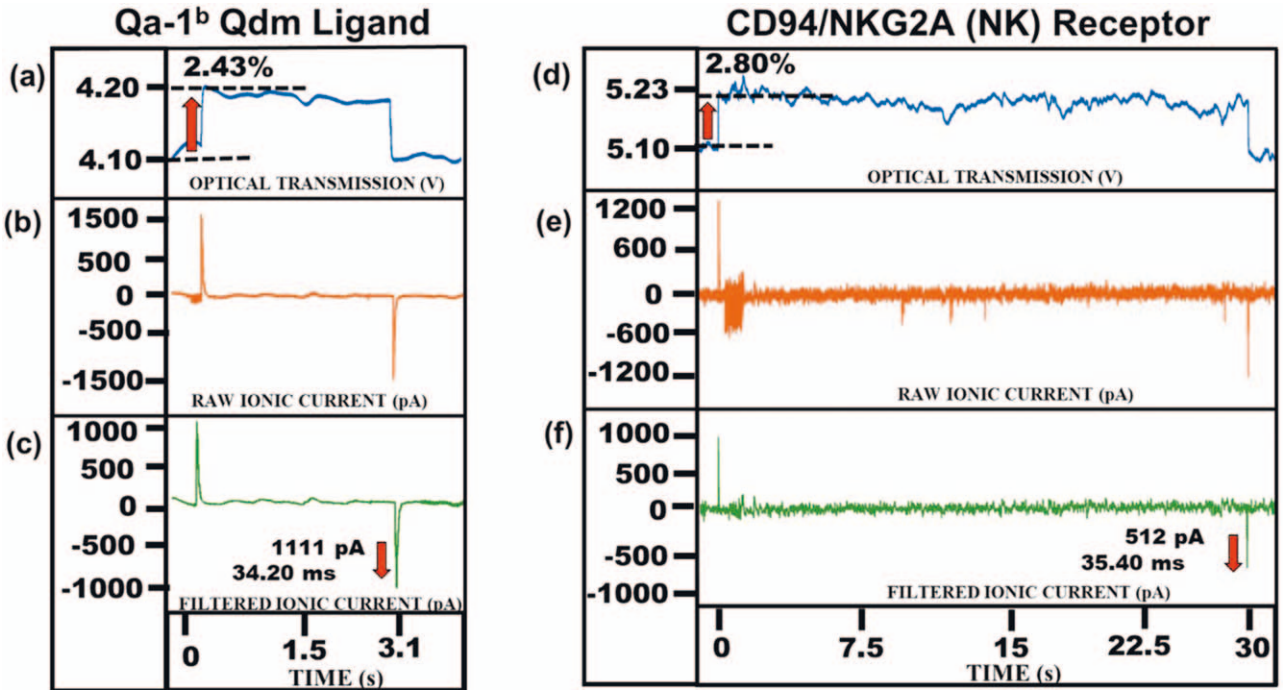

Figure 2. Time traces of individual Qdm ligand (a)–(c) and NK receptor molecules, (d)–(f). Optical transmission (a) and (d), raw ionic current (b) and (e) and low-pass filtered ionic current (c) and (f).

Table 1. Average optical and electrical metrics of ligand and receptor molecules.

Metric	Qdm ligand	NK receptor
Optical step change (%)	3.02% ± 0.37%	Group 1 = 3.04% ± 0.51% Group 2 = 5.06% ± 0.44%
Optical trap time (s)	2.69 s ± 2.71 s	Group 1 = 21.32 s ± 18.92 s Group 2 = 60.96 s ± 14.20 s
Translocation current (pA)	625.12 pA ± 246.08 pA	600.72 pA ± 277.08 pA
Translocation time (ms)	35.26 ms ± 4.42 ms	36.63 ms ± 6.15 ms

receptor [42] to compare and contrast with the SANE sensor results.

We compiled observed ligand-receptor binding duration times into histograms and natural log values of these event frequencies were determined and fitted to a linear equation to verify if they were consistent with first order off-binding kinetics, i.e. $\exp(-k_{off}{}^{*}t)$. The slope of this line corresponded to the fitted k_{off} value of the ligand-receptor bound complex.

Results

Firstly, we tested individual solutions of specific ligand and NK receptor to identify their characteristic bimodal metrics measured by the SANE sensor. This was a necessary step for subsequently distinguishing individual proteins from the complexes they formed in a mixture. Figure 2 shows typical optical, raw electrical, and low-pass filtered electrical traces for each of these reactants. The average optical and electrical metrics of these ligand and receptor molecules are listed in table 1. The NK receptor molecules showed a bimodal distribution for the optical step change, with population fractions of events consisting of single molecules (74.47% of total population, group 1) and likely agglomerates (25.53% of total population, group 2) with the two groups separating clearly in the vicinity of a 4% optical step change threshold. The optical step change magnitudes of Qdm ligands and group 1 of NK receptors were statistically indistinguishable (table 1, row 2, $p = 0.29$), but the optical trapping times of the Qdm ligands were significantly lower than those of the NK receptors (table 1, row 2, $p = 3.32 \times 10^{-9}$).

The protein molecules with higher optical step change (Qdm ligands), longer optical trapping time, or both (group 2, NK receptors) are hypothesized to represent aggregates that formed during the *in vitro* refolding protocol described above.

The average electrical data types, which included the translocation current and translocation time, were similar between the Qdm ligand and all the NK receptors (table 1). All electrical data types of Qdm ligand and NK receptor (figures 3(a) and (b)) and the equimolar mixtures of Qdm-NK receptor and GroEL-NK receptor (figures 3(c) and (d)), were pooled into histograms. Based on the distribution of the event data, the histograms were fitted to a single gaussian curve, or a sum of two gaussian curves. The overlapping histograms

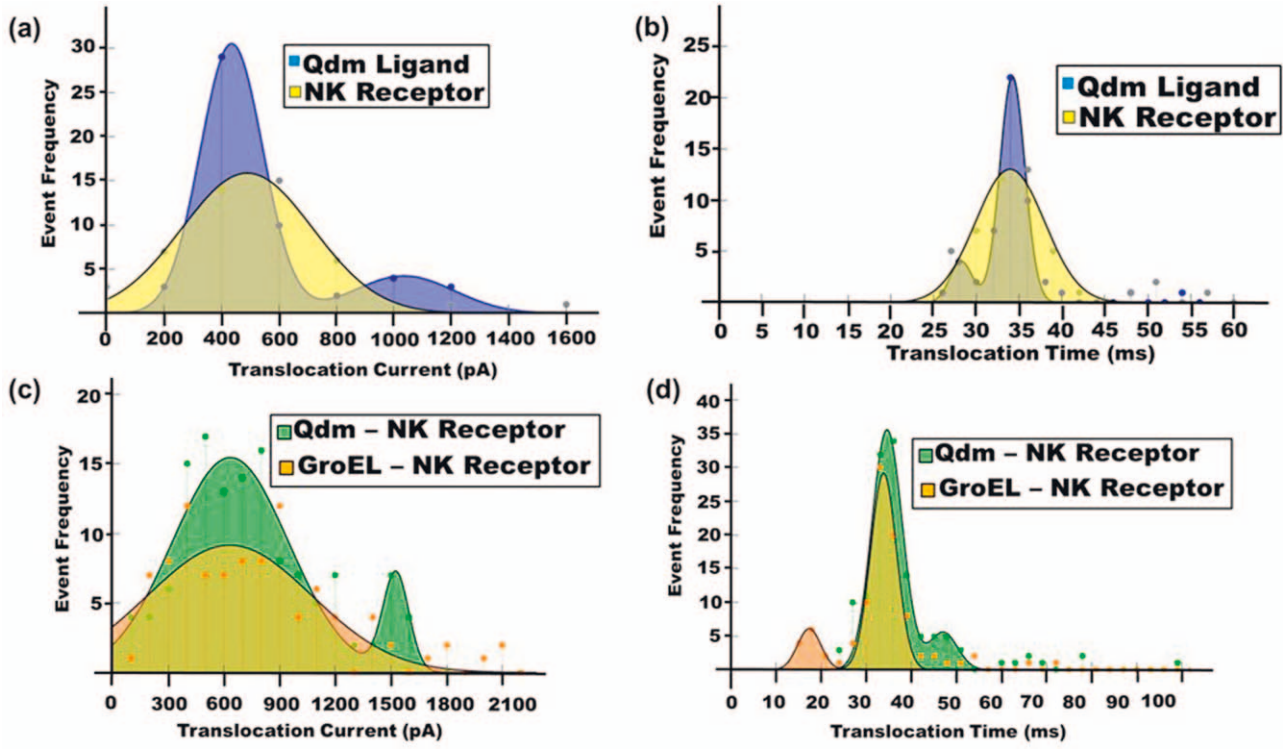

Figure 3. Histograms of translocation current and translocation time for (a), (b) individual Qdm ligand (blue) and NK receptor (yellow) and (c), (d) equimolar mixtures of Qdm-NK receptor (Green) and GroEL-NK receptor (Orange).

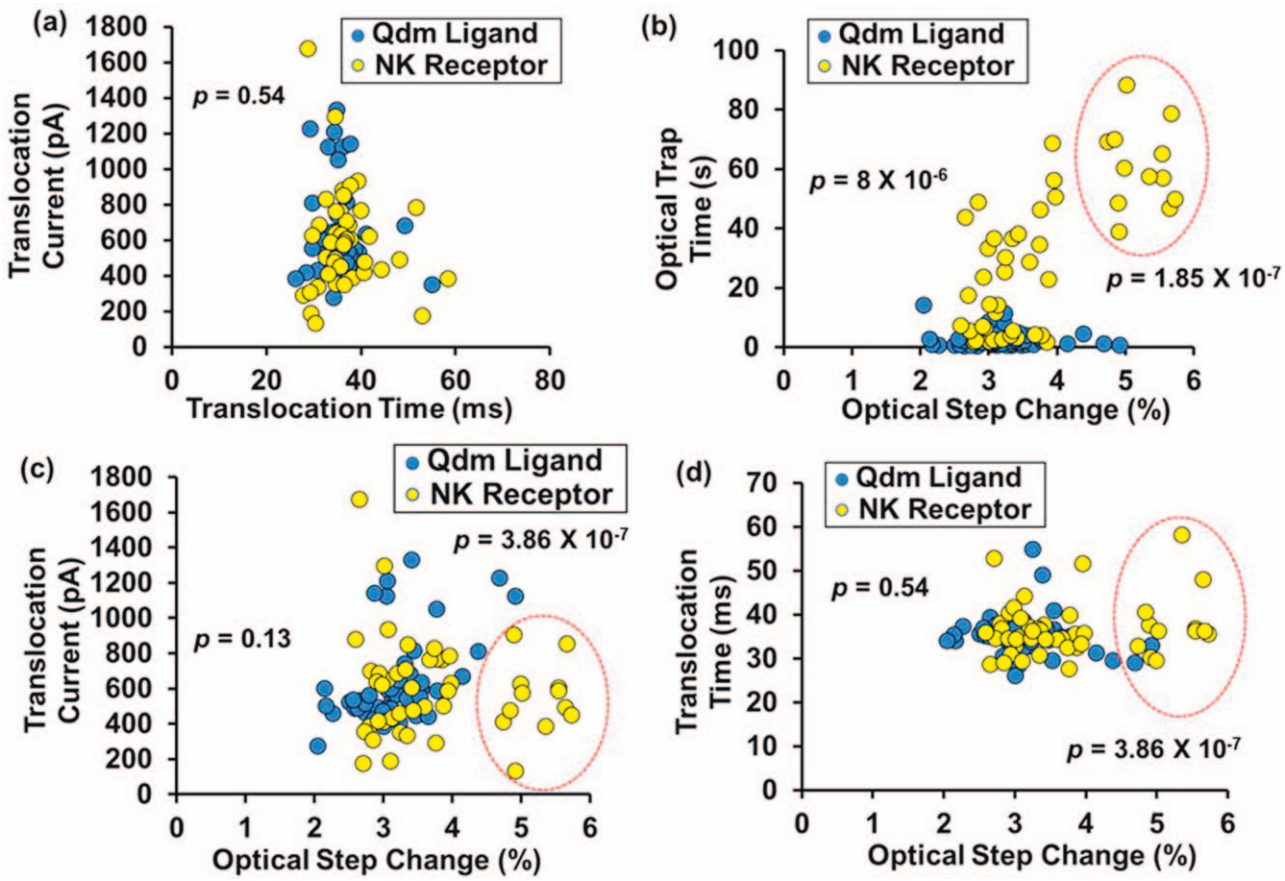

Figure 4. Event density plots comparing Qdm ligands (blue circles, $n = 51$) and both the groups of NK receptors (yellow circles, $n = 47$, group 2 is circled) for all data types. (a) Electrical metrics alone. (b) Optical metrics alone. (c), (d) Combined optical-electrical metrics. Bimodal metrics were tested for statistically significant differences using a 2s–2d KS test.

suggest that the individual ligands and their mixtures had similar electrical characteristics. A small secondary peak was seen for all event types for the Qdm ligand, possibly aggregates. The fact that all the electrical metrics plotted in figure 3 did not enable distinguishing any bound fraction in the protein mixtures suggested the need for further analyses based on bimodal electrical-optical metrics.

Figure 4 shows the compiled results for the bimodal metrics plotted in pairs for all performed measurements. Figures 4(a)–(d) show a comparison of all data types from separate experiments of Qdm ligand (blue circles) and NK receptor (yellow circles) molecules at concentrations of 300 nM in 150 mM KCl solution buffered at pH ~7.4. The difference between the pairs of optical-electrical metrics was tested using a 2s–2d KS test. For figures 4(b)–(d), both the groups of NK receptors were tested separately (group 2, inside red dotted ovals, figures 4(b)–(d)) to differentiate them from the Qdm ligands, and two sets of p values are reported in each figure. Figure 4(a) shows that electrical metrics alone could not discriminate between ligand and receptor ($p = 0.54$). Figure 4(b) clearly distinguishes between the ligand and receptor molecules, where group 2 ($p = 8.00 \times 10^{-6}$) was separable for both the optical metrics and while group 1 ($p = 1.85 \times 10^{-7}$) relied heavily on the differences in trapping times as most of the group 1 receptor events had similar optical step change values as ligands (table 1). The similarity in the optical step change of Qdm ligand to NK receptors despite their different molecular weights is possibly due to a stronger trapping of Qdm molecules due to their elongated protein structure, resulting in a shape-based increase in optical polarizability and therefore scattering strength [17] inside the DNH. The combined optical step change and electrical metrics did not show clear separation between ligands and group 1 receptors events for both the translocation current (figure 4(c), $p = 0.13$) and translocation time (figure 4(d), $p = 0.54$), but separated clearly from the group 2 receptor molecules (figures 4(c), (d), $p = 3.86 \times 10^{-7}$). Though optical step change could clearly distinguish only 25.53% of receptor (group 2) events from Qdm ligands, it presented the best available combination of metrics in this work, compared to optical trapping time, or any of the electrical metrics. Based on the results from figures 4(b)–(d), we chose to explore further the feasibility of using the optical step change metric to define a threshold and distinguish between bound and unbound receptors for all subsequent experiments.

Optical step change data pooled from equimolar mixtures of Qdm-NK receptor was distributed into histograms (figure 5) and fit to the sum of three gaussian curves. The first gaussian (left) represented a mixture of Qdm ligand and NK receptor molecules, the second one (middle) represented Qdm ligand-NK receptor complexes, and the third one (right) represented likely NK receptor agglomerates and receptor complexes with two Qdm ligands. The data could not support fitting more than three gaussian curves to resolve all five possible sub-populations. The point of minimum overlap between unbound protein populations and Qdm-NK receptor

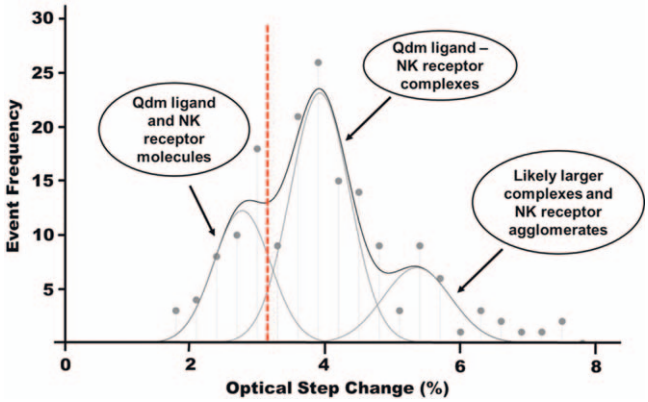

Figure 5. Histogram of optical step change for ligand-receptor (Qdm-NK receptor) equimolar mixtures. A threshold of 3.15% (red dashed line) was defined for classifying events as bound complex (middle gaussian) versus unbound ligand and receptor (left gaussian) and likely larger complexes or receptor agglomerates (right gaussian).

complexes was chosen as the threshold (3.15%) of optical step change.

Figures 6(a)–(d) represent equimolar mixtures of Qdm-NK receptor at concentrations of 600, 300, 100, and 10 nM. Applying an optical step change threshold of 3.15%, the fraction of detected Qdm-NK receptor complexes were 90.90%, 77.58%, 66.66%, and 56.52% respectively. Larger optical step changes than the threshold value and corresponding higher optical trapping times were observed among likely complex events in both figures 6(c) and (d) at concentrations of 100 nM and 10 nM compared to higher concentrations of the mixtures (600 and 300 nM). It is presumed that these events could be NK receptors agglomerates or Qdm-NK receptor complexes that had both binding sites of the NK receptor molecule occupied with Qdm ligands changing the overall charge on the molecule. Some NK receptors also show higher optical trapping time with optical step changes below the threshold. However, as these events were very few, no additional threshold criterion was applied for the discrimination of complexes in these data based on optical trapping times, although this will be evaluated further in future work.

The SANE sensor's capability to distinguish between binding of specific (Qdm) and non-specific (GroEL) ligands to NK receptor was evaluated in separate experiments. Figure 7 shows the typical time traces for both optical and electrical signals for these experiments. Figure 7(a) shows a trapping event for a Qdm-NK receptor complex, where the NK receptor was trapped at the DNH (Region A) resulting in an optical step change of 2.27% followed by binding of the Qdm ligand (Region B), resulting in a total optical step change of 4.54%. Just prior to entering Region A and Region B in figure 7(a) high frequency electrical transients were detected that are attributed to bobbing motions near the bottom of the optical trap, while proteins hover just above the nanopore [25, 26]. The total duration for that event was approximately 12 s and the complex translocated through the nanopore at the end of the trapping event. Though we

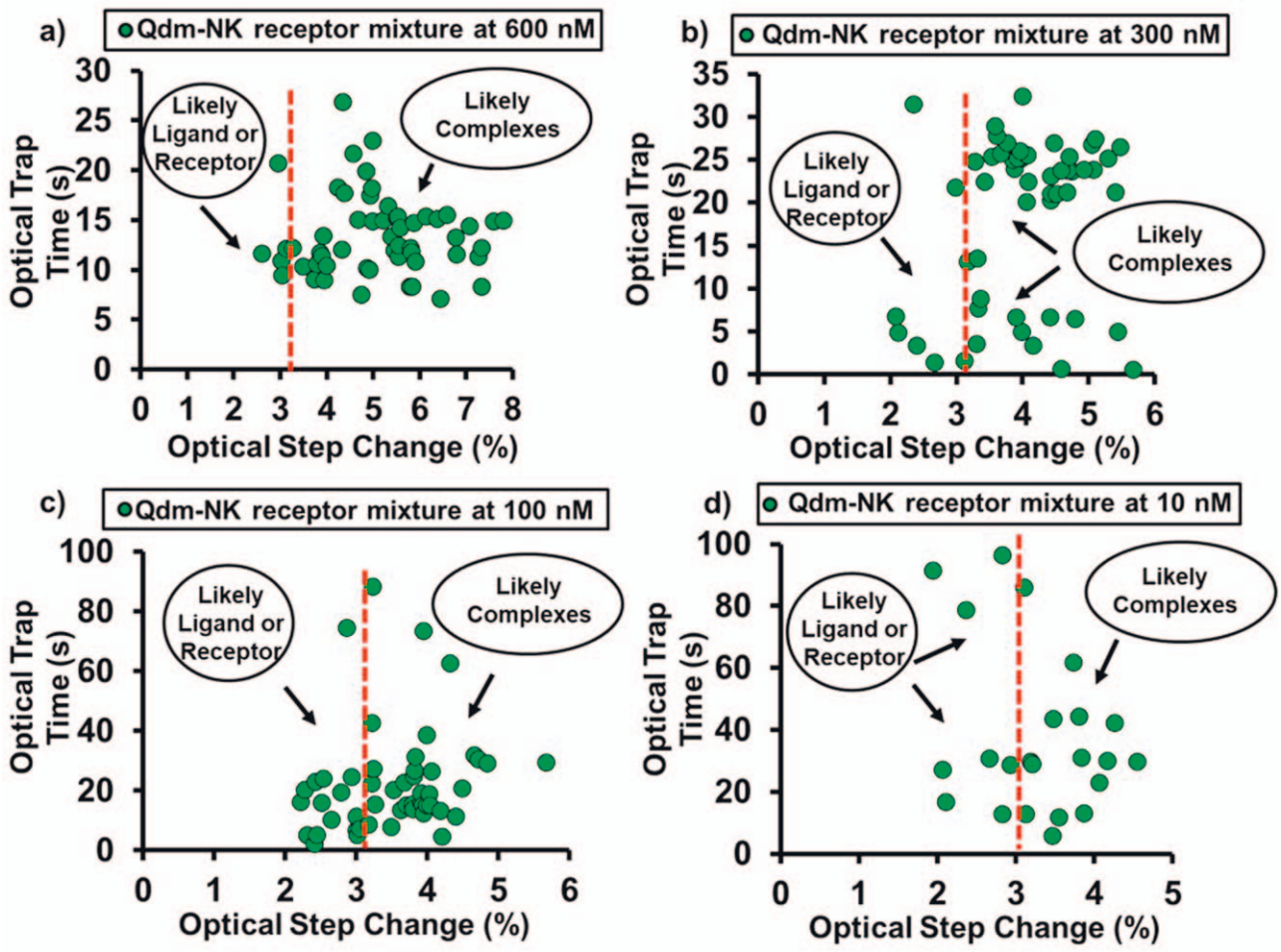

Figure 6. (a) Event scatter plots of optical metrics for equimolar mixtures of Qdm and NK receptor at (a) 600 nM (b) 300 nM, (c) 100 nM and (d) 10 nM.

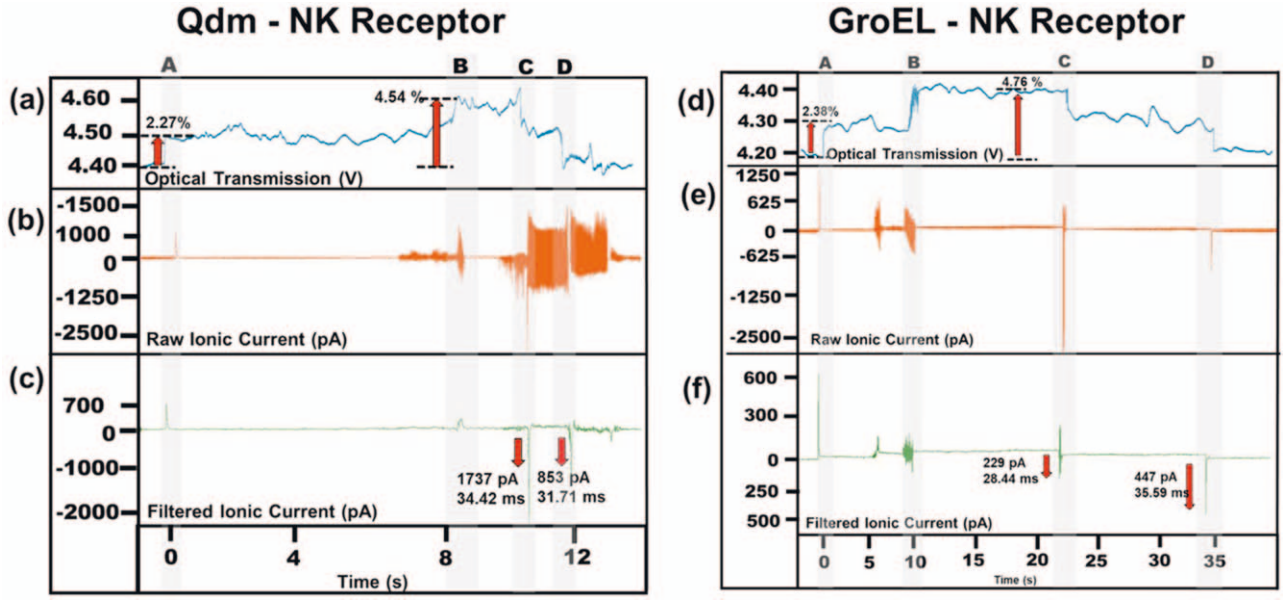

Figure 7. (a)–(c) Optical and electrical time traces from a Qdm equimolar mixture with NK receptor at 10 nM. (d)–(f) Corresponding time traces for an equimolar mixture of non-specific GroEL ligand with NK receptor at 10 nM.

Table 2. Average bimodal optical and electrical metrics of events from specific and non-specific mixtures.

Metric	Qdm-NK receptor complex	GroEL-NK receptor mixture
Optical step change (%)	4.48% ± 0.98%	3.35% ± 0.83%
Optical trap time (s)	20.99 s ± 12.38 s	33.39 s ± 24.99 s
Translocation current (pA)	808.83 pA ± 381.97 pA	824.45 pA ± 449.24 pA
Translocation time (ms)	39.09 ms ± 11.08 ms	35.89 ms ± 12.08 ms

observed two translocation events in the trace, we consider only the second one that coincides with the optical signal, confirming the bound complex exited from the trap. After applying a low-pass 20 Hz filter, the translocation event was electrically detected (figure 7(c), Region B), concurrently with an optical step change (figure 7(a), Region B), denoting a binding event between Qdm and NK receptor. After unbinding, receptor and ligand translocated through the nanopore separately, the Qdm ligand (figure 7(a), Region C) was the first to leave the optical trap followed by NK receptor (figure 7(a), Region D).

Figures 7(d)–(f) show typical optical and electrical traces from the non-specific GroEL-NK receptor mixtures. Figure 7(d) shows the trapping event of a receptor (Region A) resulting in an optical step change of 2.38%, followed by the interaction of a GroEL ligand (Region B) with the NK receptor, leading to a total optical step height change of 4.76%. In contrast, the GroEL-NK receptor binding duration lasted longer than Qdm events (figure 7(d), between Regions B and C, ∼13 s). Subsequently, the GroEL molecule tended to exit the optical trap first (figure 7(d), Region C) and translocate through the nanopore (figure 7(e), dip in electrical current, Region C), while the receptor continued to stay trapped for longer (figure 7(d), between Regions C and D, ∼12 s) before leaving the trap too (figure 7(d), Region D). Like the events from specific mixtures, bobbing motions were also observed here as high frequency electrical transients in the raw ionic current (figure 7(e), Region A and Region B) whenever a particle entered or left the optical trap.

Table 2 shows the average bimodal metrics of events from Qdm-NK receptor complexes and the GroEL-NK receptor mixture. The large amounts of variation observed in the translocation current and translocation time of Qdm-NK receptor complexes is likely due to the fact that the NK receptor is a heterodimer molecule with high flexibility in its two arms that affects the overall shape, number of sites saturated with ligands, and finally the effective surface charge on the molecule during translocation through the nanopore. The optical metrics and the translocation current of Qdm-NK receptor complexes were significantly different from free ligands or free receptors ($p < 0.05$, table 3). In addition, the translocation time of Qdm-NK receptor complexes were significantly different from free ligands ($p < 0.05$) and showed no separation with respect to free receptors ($p > 0.05$). This provides strong evidence that the binding is dynamic where the ligand-receptor binding duration is shorter and they dissociate into individual proteins before translocating through the nanopore (figures 7(a) and (d), Region C and Region D). The GroEL-NK receptor events did not show any statistically significant differences with the free receptors and were only different for their optical trapping time in comparison to free ligands ($p \ll 0.001$, table 3).

To answer the question of whether the SANE sensor can separate specific from non-specific binding, we performed measurements on equimolar mixtures of Qdm-NK receptor (specific mixture) and GroEL-NK receptor (non-specific mixture) prepared at 600, 300, 100 and 10 nM. We pooled optical-electrical metrics from experiments across all concentrations and created a scatter plot to differentiate between these mixtures as shown in figures 8(a)–(d). In these scatter plots, the 3.15% optical step change threshold was applied for these mixtures where the specific binding data (above-threshold, green circles, figure 8) was compared to the non-overlapping events of the non-specific mixture (below-threshold, orange circles, figure 8). A 2s–2d KS test was used to evaluate the differences between these mixtures. Figure 8 shows that even the optical step data that was clearly separable by optical metrics (figure 8(b), $p < 0.01$) was still not distinguishable by electrical metrics (figure 8(a), $p > 0.01$). Therefore, combinations of optical-electrical metrics (figures 8(c), (d), $p < 0.01$) provided clearest separation between the green and orange circles.

These latter data (non-specific mixture) had mixed distinguishability, with some events being clearly distinguishable from specific interactions (below-threshold optical step change, orange circles, figure 8) and others that were overlapping with them (above-threshold optical step change, pink circles, figure 9). Therefore, we considered only the overlapping data points (pink circles, figure 9) of the non-specific mixture and evaluated the differences with the specific binding data (green circles, figure 9) using the 2s–2d KS test. We found that no combination of metrics, including optical ones, separated the pink from the green circles. The fraction of optical step data overlapping between specific and non-specific interactions can be made clearly separable by further consideration of the differences in the binding time durations of the ligand-receptor interactions. Figure 10(a) shows a typical optical signature of a specific binding event, where the entry of ligand (Qdm, Region B in figure 10(a)) is seen as a rise in optical amplitude above the existing optical step change of the receptor (NK receptor, Region A in figure 10(a)). The total duration of this interaction (Region B to Region C) before the ligand left (Region C) the optical trap was considered as the effective binding duration. Qualitatively similar step changes observed in the non-specific mixtures (figure 10(b)), were used to define an effective binding duration for GroEL. The binding time of Qdm-NK receptor (3.35 s ± 2.05 s) was shorter than GroEL-NK

Table 3. The p-values from independent sample t-tests comparing molecules from each mixture type with the free ligands and receptors (significance set at $p = 0.05$).

Metric	Qdm-NK receptor complex versus Qdm ligand *(p value)*	Qdm-NK receptor complex versus NK receptor *(p value)*	GroEL-NK receptor mixture versus Qdm ligand *(p value)*	GroEL-NK receptor mixture versus NK receptor *(p value)*
Optical step change (%)	$p \ll 0.001$	$p \ll 0.001$	0.15	0.01
Optical trap time (s)	$p \ll 0.001$	$p \ll 0.001$	$p \ll 0.001$	0.66
Translocation current (pA)	0.002	$p \ll 0.001$	0.004	0.002
Translocation time (ms)	0.018	0.15	0.72	0.69

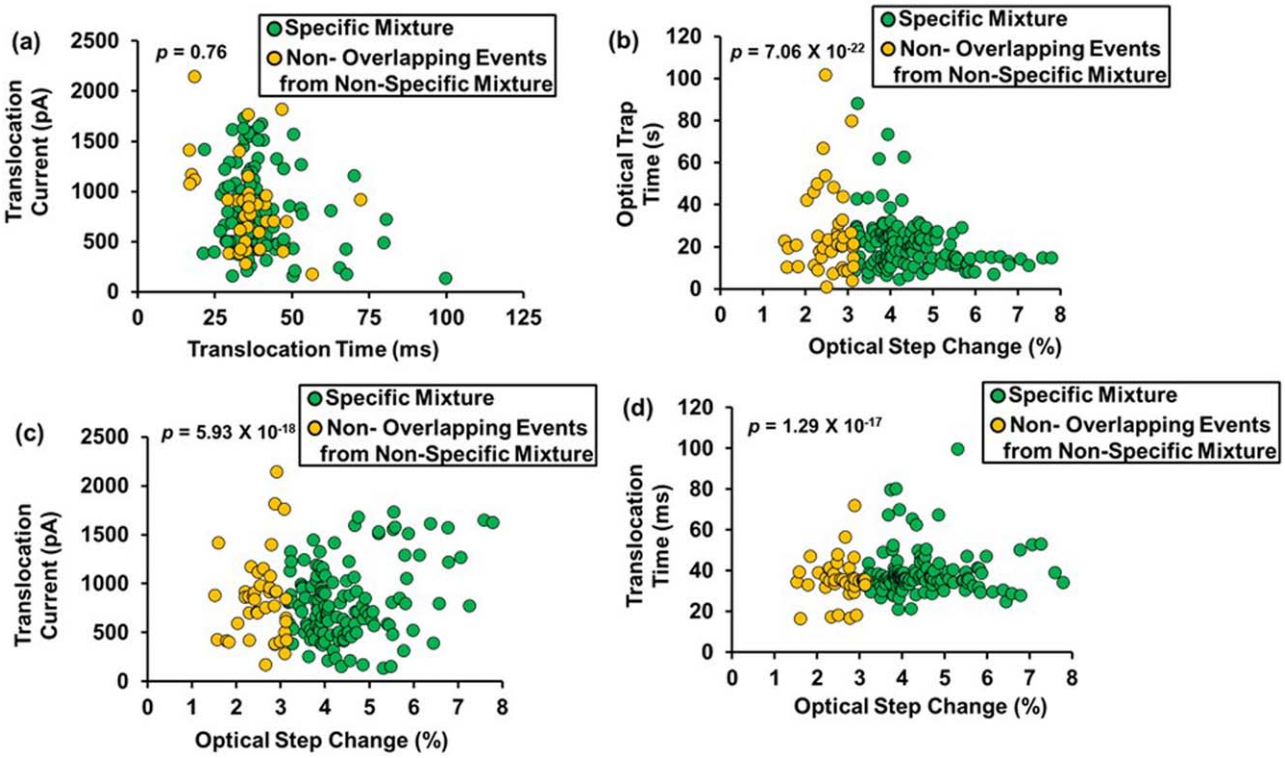

Figure 8. Event density plots comparing the specific mixture (Qdm-NK receptor, green circles ($n = 132$)) with the non-specific mixture (GroEL-NK receptor, orange circles ($n = 41$)) for all data types. (a) Electrical nanopore translocation times and translocation current for an NK receptor targeting a specific Qdm ligand and a non-specific GroEL ligand are highly overlapped. (b) Optical metrics alone. (c), (d) Event density plots comparing optical transmission data with electrical nanopore data to enable discrimination between specific and non-specific binding. Some events showed clear separation (optical step change <3.15%, orange circles) from the specific mixture. Bimodal metrics were tested for statistical differences using a 2s–2d KS test ($p < 0.01$).

receptor (14.92 s ± 6.43 s) with clear statistical significance ($p < 0.05$), where binding durations extracted from the optical data were pooled from experiments across all concentrations. Figure 10(c) shows the corresponding total optical step change data for all these binding events as an event frequency histogram. In figure 10(d), we plotted the data overlapping in figure 10(c) for optical step change of non-specific and specific mixtures as a function of their binding duration metrics. Figure 10(d) indicated that plotting optical step change versus binding duration could help sperate specific from non-specific interactions.

To further verify the SANE sensor's ability to use binding duration as an additional metric for separating specific from non-specific interactions, we also plotted optical step change versus the natural log of the event frequency, which would be proportional to $\ln(\exp(-k_{off}^{*}t))$, i.e. a linear slope for first order kinetics. The inverse of this slope represented the mean residence time of this binding interaction, $k_{off} = 1/(\text{mean residence time})$. Figure 10(e) shows that Qdm-NK receptor binding duration values followed a log-linear dependence. The slope of the line, or k_{off}, was $0.403\ s^{-1}$, which is consistent with the known value of $0.42\ s^{-1}$ (kinetic data averaged over 2–5 experiments with several batches of refolded protein) for a human analogue of Qdm [38]. In contrast, figure 10(f) shows that the GroEL binding durations to NK receptor did not have any discernible pattern, consistent with non-specific interactions.

A unique advantage of this nanosensor is that it enables detection of low-affinity interactions, which require high protein amounts in bulk solution, to be observed at much lower concentrations. The key to this technological ability is an electric-field-induced protein crowding within a nanoscopic optical trap volume immediately over the SANE sensor (figure 11(a)). Proteins can interact at much higher concentrations locally, just before translocating through the sensor, which enabled us to use very low amounts of ligands to detect a much higher bound fraction than would have been predicted at that concentration for bulk solution measurements. Figure 11(b) shows the bound fraction for Qdm-NK receptor complexes detected by the SANE sensor as a function of concentration in equimolar mixtures, using the 3.15% optical step threshold criterion, as in figure 5. At the lowest concentration tested of 10 nM, the SANE sensor detected bound events by a factor of >500 higher than the bound fraction estimated from free solution conditions based on the K_D value reported in literature (17 ± 2.8 μM) [42]. An important clue to help explain the increased bound fraction can be seen in figure 11(c), where at the very beginning of an experimental run it takes several seconds with no events detected before individual proteins and protein complexes are detected, one after the other. These data suggest that proteins converge to the optical trap of the SANE sensor and can interact locally before they have a chance to translocate through the nanopore below.

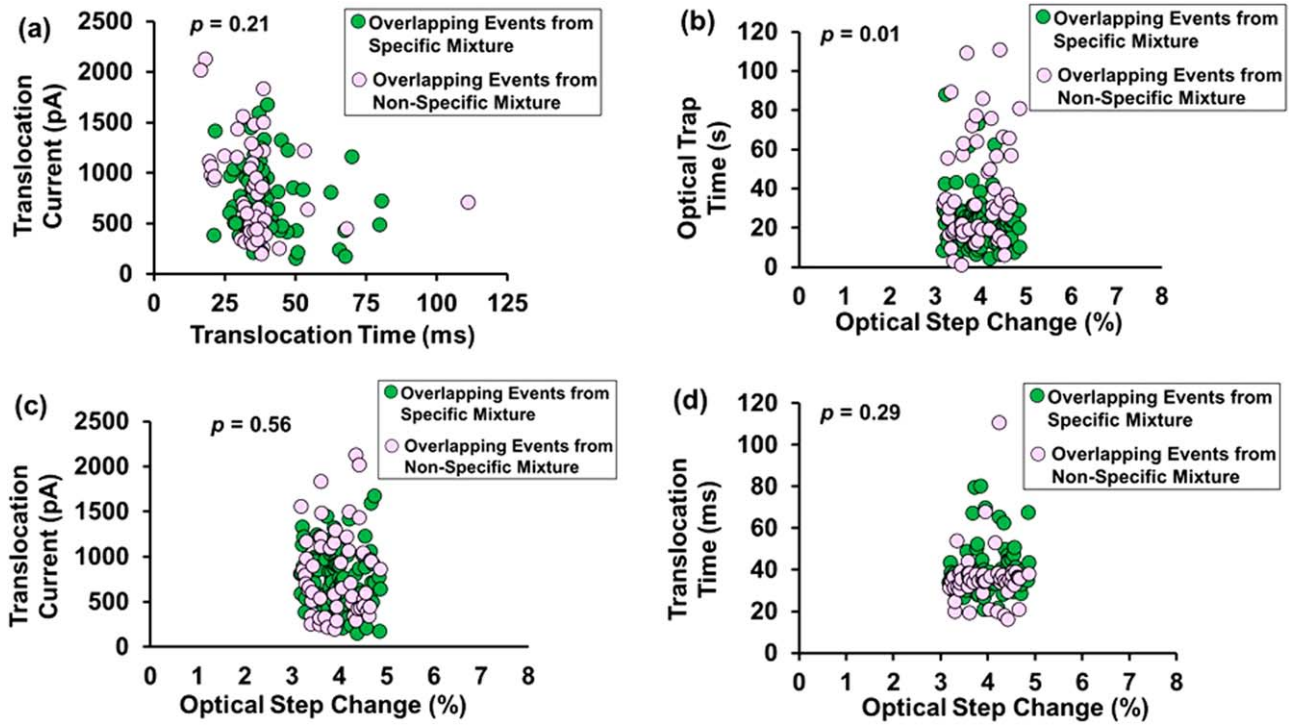

Figure 9. Event density plots comparing the overlapping events of non-specific mixture (GroEL-NK receptor, pink circles ($n = 55$)) with specific mixture (Qdm-NK receptor, green circles ($n = 98$)) for all data types. The overlapping events (optical step change >3.15% in non-specific mixture) were identified as non-specific binding through ligand-receptor binding duration, to be discussed below. (a) Electrical nanopore translocation times and translocation current for an NK receptor targeting a specific Qdm ligand and a non-specific GroEL ligand are highly overlapped. (b) Optical metrics alone. (c), (d) Event density plots comparing optical transmission data with electrical nanopore data to enable discrimination between specific and non-specific binding. Bimodal metrics were tested for statistical differences using a 2s–2d KS test ($p < 0.01$).

Discussion

This work presents the use of a bimodal optical-electrical SANE sensor to quantify low-affinity protein interactions and discriminate between individual free ligand and free receptor molecules, and complexes formed by receptors through interaction with specific or non-specific ligands. Optical data (optical amplitude change and trapping duration) and electrical data (translocation current and translocation time) were recorded to differentiate between these individual molecules and their various binding interactions. The NK receptor molecules presented a bimodality in their optical metrics representing two populations, where about ∼25% of events had a significantly larger optical step change and longer trapping times (group 2). A few Qdm ligands also displayed similar behavior along with higher translocation currents. We attribute all these events as agglomerates formed during the *in vitro* protein refolding protocol described above. Like in our previous work on high-affinity protein interactions [26], using electrical metrics alone did not help in separating individual ligands from both the receptor groups (figures 3(a), (b), 4(a)).

Moreover, Qdm ligands with smaller molecular weight than NK receptors had similar optical step change mean value (table 1, $p > 0.05$) as 74.74% of the receptor molecules (group 2, figure 4(b)), but the optical trapping times were shorter ($p \ll 0.05$). This modulation in optical trapping behavior is hypothesized to be an effect of stronger optical trapping due to the shape of a molecule in the optical trap than just simple molecular weight based trapping behavior that assumes spherical proteins. Previous studies have shown increased optical polarizability [17] based on the shape of the protein molecule leading to a stronger trapping and increased light transmission through the DNH for more oblong-shape proteins. We hypothesize that a similar optical polarizability phenomenon is causing the oblong shape of Qdm ligands [42] to have matched optical step change as NK receptors (group 1). We tested the optical metrics, optical step change (figures 4(c), (d)) and optical trapping time (not shown for brevity) in combination with electrical metrics for bimodal comparison and found that optical step change provided a clearer separation. Based on these findings we selected optical step change, the change in optical transmission intensity through the DNH structure of the SANE sensor, as the metric to identify bound complexes.

We used a 3.15% optical step change threshold, calculated as a point of minimum overlap (red dashed line, figure 5) from the gaussian curve fit (figure 5) to the histogram of pooled events from Qdm-NK receptor mixtures. Using this as a definitive metric, we separated Qdm ligand-NK receptor complexes (middle gaussian, beyond the red dashed line, figure 5) from a mixture free ligands and free receptors (left gaussian, figure 5). Events beyond 4.8% optical step change were separated in into a third gaussian (right,

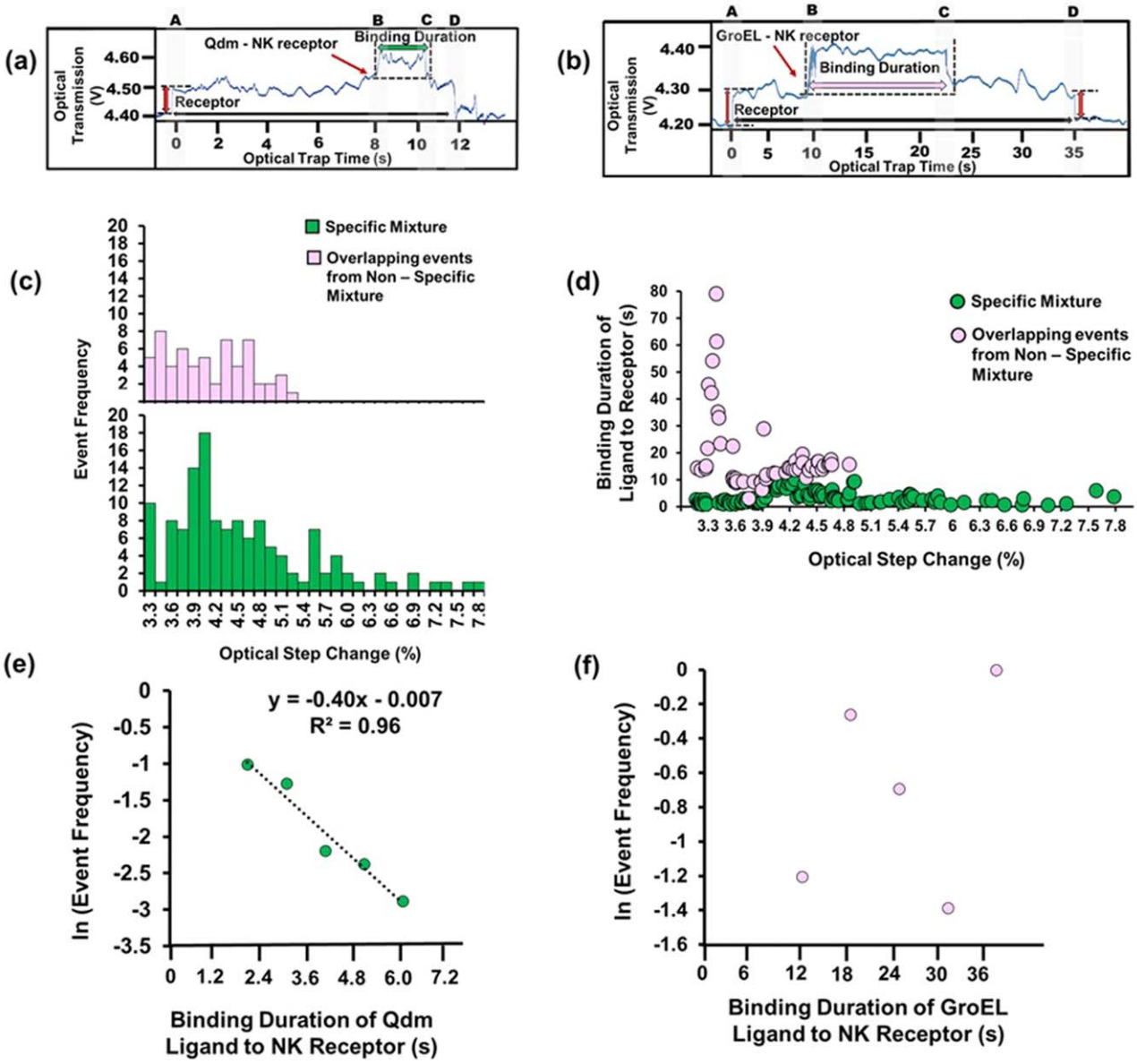

Figure 10. (a) A typical binding duration observed for low-affinity (μM) interactions of Qdm-NK receptor complexes at 10 nM concentration ($\sim$2 s). (b) Typical binding interaction of Groel-NK receptor at 10 nM concentration ($\sim$13 s). (c) Event frequency histograms of optical step change for all the specific binding events (green columns) and overlapping events (pink columns) from non-specific mixture. (d) Scatter plot separating the non-specific mixture events (pink circles, $n = 55$) from specific binding events (green circles, $n = 132$) based on binding duration and optical step change. Natural log plot of event frequency of ligand-receptor binding interaction duration for (e) specific mixture and (f) non-specific mixture. In contrast to (e), the data could not be fit to a linear curve in (f). The slope of the line equation is the k_{off}.

figure 5) consisting of NK receptor agglomerates and likely complexes with both the binding sites of receptor saturated with two Qdm ligands. Though we could not show all the five sub-populations in the gaussian fitting, we were able to clearly distinguish all the Qdm-NK receptor complexes based on their ligand-receptor binding duration in subsequent analyses (figure 10) discussed below.

Another interesting observation was the apparent increase of the Qdm-NK receptor complex translocation current, reflective of surface charge, (table 2) and its significant differences compared to its two constituent molecules (table 3). Previous reports have shown that protein interactions can lead to changes in the overall charge of the bound complex due to conformational changes [16]. However, the slowing down of translocations by the opposing optical force may have contributed to minimizing the effect of any charge differences would have on the translocation times for these molecules.

In addition to detecting and characterizing the individual molecules and likely complexes, the SANE sensor was also tested for its ability to differentiate specific binding events (Qdm-NK receptor complexes above the optical threshold of 3.15%) from non-specific interactions between the same NK receptor molecule and a non-targeting ligand (GroEL). Figure 8(a) shows that event data of non-specific mixture (orange circles, figure 8) could not provide clear separation

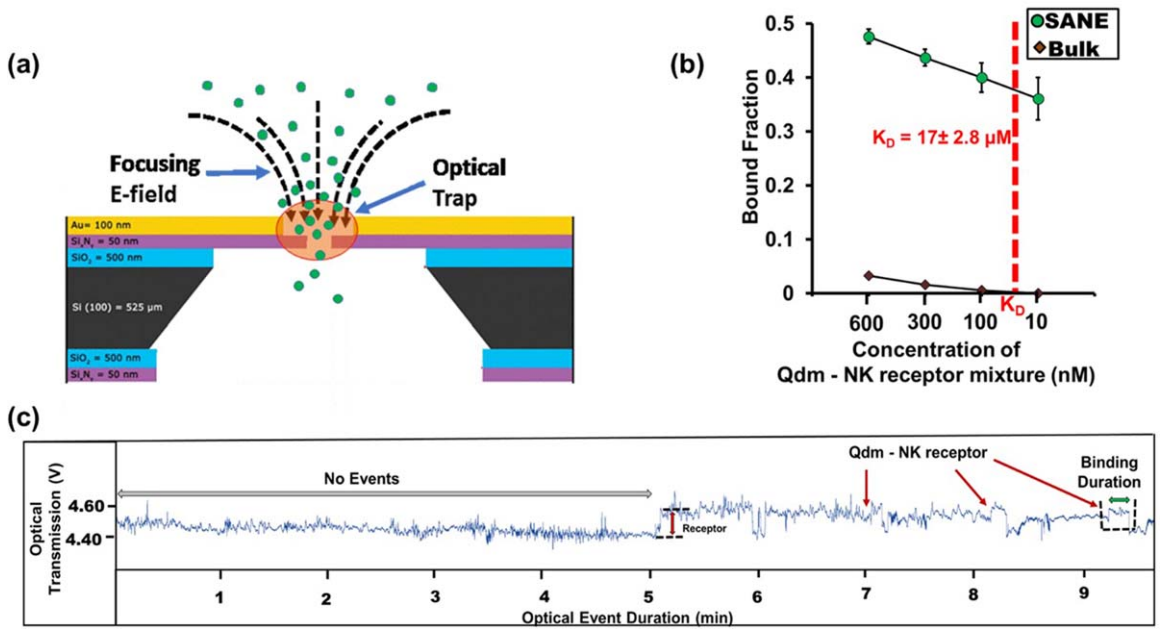

Figure 11. (a) Schematic of the protein crowding effect created by the applied electric field immediately over the SANE sensor. (b) The observed Qdm-NK receptor bound fraction is significantly higher than corresponding values at the same bulk Qdm-NK receptor concentrations, due to the sensor-induced protein crowding. (c) Zoomed out time-series plot showing no trapping events for several seconds at the beginning of an experiment.

using electrical metrics alone while the optical alone (figure 8(b)) or optical-electrical metrics (figures 8(c), (d)) could provide clear separation. The non-specific ligand (GroEL) was selected to have similar molecular weight to the specific (Qdm) ligand, and we also found through our experiments (not shown for brevity) that its electrical characteristics were not significantly different from either of the free molecules (ligands or receptors, $p > 0.05$). As a result, some of the events from the non-specific mixture (figures 9(a)–(d), pink circles) could not be separated from the Qdm-NK receptor complexes (figures 9(a)–(d), green circles) using any combination of the metrics. We therefore subsequently explored using binding duration (figure 10(d)) as an additional metric to optical step change to help separate specific from non-specific binding.

An additional advantage of the SANE sensor is its ability to detect low-affinity (μM K_D range) binding durations resulting from fast dissociation kinetics that are difficult to detect by conventional plasmon resonance systems [37]. It was previously reported that fast translocation times for antigen–antibody complexes make it difficult for them to be detected through nanopores [16], as reactants are in the bound state infrequently at low affinities. Also, molecules can be trapped optically for prolonged times, limiting the detection of these interactions [17, 43]. Using the SANE sensor, the presence of the electric field limits the optical trapping time duration and reduces the probability to trap multiple molecules within the sensing volume. The importance of slowing down a SSNP event allows more time for low-affinity ligand-receptor interactions to occur in the optical trap, thus increasing the probability of detecting such events translocating through the SSNP. Therefore, we were able to estimate the binding duration of ligand to receptor from the optical transmission signals (figures 10(a) and (b)) which aided in the discrimination of overlapping events (pink circles, figures 9(a)–(d)) of non-specific mixture from the Qdm-NK receptor bound complexes (figure 10(d)). Therefore, the SANE sensor helped confirm the presence of non-specific binding, by being able to measure simultaneously optical step intensity changes and binding duration data.

Furthermore, the time interval distribution resulting from the binding duration data did not show any discernible patterns for GroEL-NK receptor interactions (figure 10(f)), in contrast to specific Qdm-NK receptor interactions (figure 10(e)) that were consistent with a single-exponent off-binding interval distribution and led to the estimation of k_{off}. It is likely that the bound complex gets pulled by the optical field gradient [18] (figure 10(a), Region C) while it is forced to translocate. It is possible that this pulling effect could increase the apparent k_{off} value compared to bulk solution conditions. However, the reported value of $k_{\text{off}} = 0.42\ \text{s}^{-1}$ for a human analogous [44, 45] compared to the $k_{\text{off}} = 0.403\ \text{s}^{-1}$ measured in this study indicates that this effect may not be significant.

In addition to detecting specific binding, one of the potential advantages of the SANE sensor is that molecules can stay within the optical trap for many seconds before the competing electrical bias forces them through the nanopore. This arrangement does not only allow for much prolonged electrical sensing of molecules, as we have previously reported [26], but also presents an interesting molecular crowding effect (figure 11(a)) that was particularly useful for the low-affinity protein interactions studied here. As the electrical field syphoned proteins towards the center of the

SANE sensor, we hypothesize that a 'traffic jam' occurred as the optical trap reduced the underlying nanopore throughput. The lack of detected events at the very beginning of experiments (figure 11(c)), while proteins were converging to the SANE sensor, is consistent with this hypothesis. Even though reduction of throughput is generally a disadvantage, in this case it provided the advantage of enabling much higher collision frequencies between reactant proteins within a small volume over the nanopore. We speculate that it is this crowding effect that enabled us to detect a significant bound fraction at reactant concentrations that were lower by up to a factor of over 500 below the free solution K_D.

Importantly, given that typical binding durations for Qdm-NK receptor complexes at 10 nM concentration (∼2 s) were much shorter than the NK trapping duration (∼12 s), one can deduce that those binding events must have occurred mostly within this crowding environment near the SANE sensor. In contrast, if the ligand-receptor complexes formed further afield from the SANE sensor, they would likely unbind before having a chance to translocate though the nanopore. Being able to detect low-affinity interactions not near their K_D (17 μM in this case), but at much lower concentrations (down to 10 nM in this work) offers good promise for testing biologically relevant interactions with great savings in the protein amounts needed. Furthermore, the constant electrical bias directs protein reactants towards the SANE sensor, which significantly reduces the time one has to wait for a single molecule event to be detected at low protein concentrations compared to relying on diffusion alone to bring proteins to the optical trap.

Use of electrical metrics alone (figures 3(c), (d)) could not discriminate the presence of bound complexes. Comparison with the optical data in figure 5 suggests that these same data points also had the largest optical step changes, consistent with a larger protein complex mass, i.e. aggregates. In contrast, use of optical metrics in figure 5, clearly suggested a bound fraction for Qdm-NK receptor complexes (∼80%). We interpret these results to mean that optical metrics offer higher sensitivity compared to electrical ones, enabling detection of ligand binding to NK receptors. The higher sensitivity of optical metrics performed by the SANE sensor, versus electrical ones, is consistent with our prior findings on high-affinity anti-RAH antibody binding to RAH ligands [26]. A noteworthy contribution of this work is that it shows the feasibility of using optical step changes to identify binding and unbinding events (figure 11(c)) for low-affinity (μM range) interactions occurring in the SANE sensor as an additional optical metric to separate clearly complexes from monomers, agglomerates and non-specific interactions.

Conclusion

In this work, we have demonstrated the feasibility of using a bimodal SANE senor to quantify low-affinity kinetics between specific ligand-receptor interactions. Optical and electrical metrics from the concurrent bimodal signals were used to differentiate specific from non-specific binding. Our results suggest the feasibility of estimating the dissociation rate (k_{off}) of low-affinity interactions at concentrations significantly below their free solution K_D. With further characterization and scale-up considerations, the SANE sensor could be used as a potential screening tool for receptor-ligand interactions at much lower reactant concentrations compared to what is possible with current methods, which presents significant potential savings in the purified protein amounts needed to perform binding assays, while also enabling enhanced detection of non-specific binding.

Acknowledgments

We thank Mr Soeren Eyhusen and Mr Chuong Huynh for permitting us with the access and providing technical guidance on focused ion beam milling at the Zeiss ORION NanoFab facility in Peabody, MA. We are also thankful to all the engineers and staff at the Shimadzu Institute Nanotechnology Research Center at the University of Texas at Arlington for their support and guidance. This work was supported through a Pilot Research Program for Interdisciplinary Collaboration funded by the Vice-President of Research Office of the University of Texas at Arlington. The authors acknowledge the financial support from the National Cancer Institute (1R21CA240220-01A1), the National Heart, Lung, and Blood Institute (NIH T32 HL134613) for Elizabeth Urquhart (née Lyde) and the National Science Foundation (CBET#2022398 and CBET#2022374). The content is solely the responsibility of the authors and does not necessarily represent the official views of the National Institutes of Health.

ORCID iDs

Sai Santosh Sasank Peri https://orcid.org/0000-0002-7224-9433
Muhammad Usman Raza https://orcid.org/0000-0003-4276-5573
Min Jun Kim https://orcid.org/0000-0002-0819-1644

References

[1] Spitzberg J D, Zrehen A, van Kooten X F and Meller A 2019 Plasmonic-nanopore biosensors for superior single-molecule detection *Adv. Mater.* **31** e1900422
[2] Neuman K C and Nagy A 2008 Single-molecule force spectroscopy: optical tweezers, magnetic tweezers and atomic force microscopy *Nat. Methods* **5** 491–505
[3] Dekker C 2007 Solid-state nanopores *Nat. Nanotechnol.* **2** 209–15
[4] Ilyas A, Asghar W, Allen P B, Duhon H, Ellington A D and Iqbal S M 2012 Electrical detection of cancer biomarker using aptamers with nanogap break-junctions *Nanotechnology* **23** 275502
[5] Yuan Z, Wang C, Yi X, Ni Z, Chen Y and Li T 2018 Solid-state nanopore *Nanoscale Res. Lett.* **13** 56

[6] Trenevska I, Li D and Banham A H 2017 Therapeutic antibodies against intracellular tumor antigens *Front. Immunol.* **8** 1001

[7] Butler T Z, Pavlenok M, Derrington I M, Niederweis M and Gundlach J H 2008 Single-molecule DNA detection with an engineered MspA protein nanopore *Proc. Natl Acad. Sci. USA* **105** 20647–52

[8] Varongchayakul N, Song J, Meller A and Grinstaff M W 2018 Single-molecule protein sensing in a nanopore: a tutorial *Chem. Soc. Rev.* **47** 8512–24

[9] Smeets R M, Keyser U F, Krapf D, Wu M-Y, Dekker N H and Dekker C 2006 Salt dependence of ion transport and DNA translocation through solid-state nanopores *Nano Lett.* **6** 89–95

[10] Freedman K J, Haq S R, Edel J B, Jemth P and Kim M J 2013 Single molecule unfolding and stretching of protein domains inside a solid-state nanopore by electric field *Sci. Rep.* **3** 1638

[11] Gershow M and Golovchenko J A 2007 Recapturing and trapping single molecules with a solid-state nanopore *Nat. Nanotechnol.* **2** 775–9

[12] Kowalczyk S W, Hall A R and Dekker C 2009 Detection of local protein structures along DNA using solid-state nanopores *Nano Lett.* **10** 324–8

[13] Plesa C, Kowalczyk S W, Zinsmeester R, Grosberg A Y, Rabin Y and Dekker C 2013 Fast translocation of proteins through solid state nanopores *Nano Lett.* **13** 658–63

[14] Talaga D S and Li J 2009 Single-molecule protein unfolding in solid state nanopores *J. Am. Chem. Soc.* **131** 9287–97

[15] Saharia J, Bandara Y N D, Goyal G, Lee J S, Karawdeniya B I and Kim M J 2019 Molecular-level profiling of human serum transferrin protein through assessment of nanopore-based electrical and chemical responsiveness *ACS Nano* **13** 4246–54

[16] Han A, Creus M, Schürmann G, Linder V, Ward T R, De Rooij N F and Staufer U 2008 Label-free detection of single protein molecules and protein−protein interactions using synthetic nanopores *Anal. Chem.* **80** 4651–8

[17] Pang Y and Gordon R 2012 Optical trapping of a single protein *Nano Lett.* **12** 402–6

[18] Juan M L, Gordon R, Pang Y, Eftekhari F and Quidant R 2009 Self-induced back-action optical trapping of dielectric nanoparticles *Nat. Phys.* **5** 915

[19] Pang Y and Gordon R 2011 Optical trapping of 12 nm dielectric spheres using double-nanoholes in a gold film *Nano Lett.* **11** 3763–7

[20] Kumar L, Lesuffleur A, Hughes M and Gordon R 2006 Double nanohole apex-enhanced transmission in metal films *Appl. Phys.* B **84** 25

[21] Burkhartsmeyer J, Wang Y, Wong K S and Gordon R 2020 Optical trapping, sizing, and probing acoustic modes of a small virus *Appl. Sci.* **10** 394

[22] Gordon R 2019 Biosensing with nanoaperture optical tweezers *Opt. Laser Technol.* **109** 328–35

[23] Jonsson M P and Dekker C 2013 Plasmonic nanopore for electrical profiling of optical intensity landscapes *Nano Lett.* **13** 1029–33

[24] Li Y, Nicoli F, Chen C, Lagae L, Groeseneken G, Stakenborg T, Zandbergen H W, Dekker C, Van Dorpe P and Jonsson M P 2015 Photoresistance switching of plasmonic nanopores *Nano Lett.* **15** 776–82

[25] Raza M U, Peri S S S, Ma L C, Iqbal S M and Alexandrakis G 2018 Self-induced back action actuated nanopore electrophoresis (SANE) *Nanotechnology* **29** 435501

[26] Peri S S S, Sabnani M K, Raza M U, Ghaffari S, Gimlin S, Wawro D D, Lee J S, Kim M J, Weidanz J and Alexandrakis G 2019 Detection of specific antibody-ligand interactions with a self-induced back-action actuated nanopore electrophoresis sensor *Nanotechnology* **31** 085502

[27] Shi X, Verschueren D, Pud S and Dekker C 2018 Integrating sub-3 nm plasmonic gaps into solid-state nanopores *Small* **14** 1703307

[28] Shi X, Verschueren D V and Dekker C 2018 Active delivery of single DNA molecules into a plasmonic nanopore for label-free optical sensing *Nano Lett.* **18** 8003–10

[29] Verschueren D, Shi X and Dekker C 2019 Nano-optical tweezing of single proteins in plasmonic nanopores *Small Methods* **3** 1800465

[30] Verschueren D V, Pud S, Shi X, De Angelis L, Kuipers L and Dekker C 2018 Label-free optical detection of DNA translocations through plasmonic nanopores *ACS Nano* **13** 61-70

[31] Wawro D, Zimmerman S, Magnusson R, Koulen P and Farghaly S A 2012 Photonic sensor system for screening serum biomarker proteins in ovarian cancer *Ovarian Cancer: Basic Science Perspective* vol 8090 (Rijeka, Croatia: InTech) 51-66

[32] Brooks A G, Posch P E, Scorzelli C J, Borrego F and Coligan J E 1997 NKG2A complexed with CD94 defines a novel inhibitory natural killer cell receptor *J. Exp. Med.* **185** 795–800

[33] Vance R E, Kraft J R, Altman J D, Jensen P E and Raulet D H 1998 Mouse CD94/NKG2A is a natural killer cell receptor for the nonclassical major histocompatibility complex (MHC) class I molecule Qa-1b *J. Exp. Med.* **188** 1841–8

[34] Kraft J R, Vance R E, Pohl J, Martin A M, Raulet D H and Jensen P E 2000 Analysis of Qa-1bPeptide binding specificity and the capacity of Cd94/Nkg2a to discriminate between Qa-1-peptide complexes *J. Exp. Med.* **192** 613–24

[35] Lo W F, Ong H, Metcalf E S and Soloski M J 1999 T cell responses to gram-negative intracellular bacterial pathogens: a role for CD8 + T cells in immunity to Salmonella infection and the involvement of MHC class Ib molecules *J. Immunol.* **162** 5398–406

[36] Lo W F, Woods A S, DeCloux A, Cotter R J, Metcalf E S and Soloski M J 2000 Molecular mimicry mediated by MHC class Ib molecules after infection with gram-negative pathogens *Nat. Med.* **6** 215–8

[37] Kaiser B K, Barahmand-pour F, Paulsene W, Medley S, Geraghty D E and Strong R K 2005 Interactions between NKG2x immunoreceptors and HLA-E ligands display overlapping affinities and thermodynamics *J. Immunol.* **174** 2878–84

[38] Valés-Gómez M, Reyburn H T, Erskine R A, López-Botet M and Strominger J L 1999 Kinetics and peptide dependency of the binding of the inhibitory NK receptor CD94/NKG2-A and the activating receptor CD94/NKG2-C to HLA-E *EMBO J.* **18** 4250–60

[39] Ghorbanzadeh M, Jones S, Moravvej-Farshi M K and Gordon R 2017 Improvement of sensing and trapping efficiency of double nanohole apertures via enhancing the wedge plasmon polariton modes with tapered cusps *ACS Photonics* **4** 1108–13

[40] Garboczi D N, Hung D T and Wiley D C 1992 HLA-A2-peptide complexes: refolding and crystallization of molecules expressed in *Escherichia coli* and complexed with single antigenic peptides *Proc. Natl Acad. Sci. USA* **89** 3429–33

[41] Wheaton S and Gordon R 2015 Molecular weight characterization of single globular proteins using optical nanotweezers *Analyst* **140** 4799–803

[42] Zeng L, Sullivan L C, Vivian J P, Walpole N G, Harpur C M, Rossjohn J, Clements C S and Brooks A G 2012 A structural basis for antigen presentation by the MHC class Ib molecule, Qa-1b *J. Immunol.* **188** 302–10

[43] Kotnala A, DePaoli D and Gordon R 2013 Sensing nanoparticles using a double nanohole optical trap *Lab Chip* **13** 4142–6

[44] Lin J J Y, Low-Nam S T, Alfieri K N, McAffee D B, Fay N C and Groves J T 2019 Mapping the stochastic sequence of individual ligand-receptor binding events to cellular activation: T cells act on the rare events *Sci. Signal* **12** eaat8715

[45] Yousefi O S, Guenther M, Hoerner M, Chalupsky J, Wess M, Brandl S M, Smith R W, Fleck C, Kunkel T and Zurbriggen M D 2019 Optogenetic control shows that kinetic proofreading regulates the activity of the T cell receptor *eLife* **8** e42475